MATERIALS SCIENCE

Interfacial tuning of chiral magnetic interactions for large topological Hall effects in $LaMnO_3/SrIrO_3$ heterostructures

Elizabeth Skoropata[1]*, John Nichols[1]*†, Jong Mok Ok[1], Rajesh V. Chopdekar[2], Eun Sang Choi[3], Ankur Rastogi[1], Changhee Sohn[1], Xiang Gao[1], Sangmoon Yoon[1], Thomas Farmer[4]‡, Ryan D. Desautels[4], Yongseong Choi[5], Daniel Haskel[5], John W. Freeland[5], Satoshi Okamoto[1], Matthew Brahlek[1], Ho Nyung Lee[1]§

Chiral interactions in magnetic systems can give rise to rich physics manifested, for example, as nontrivial spin textures. The foremost interaction responsible for chiral magnetism is the Dzyaloshinskii-Moriya interaction (DMI), resulting from inversion symmetry breaking in the presence of strong spin-orbit coupling. However, the atomistic origin of DMIs and their relationship to emergent electrodynamic phenomena, such as topological Hall effect (THE), remain unclear. Here, we investigate the role of interfacial DMIs in 3*d*–5*d* transition metal-oxide-based $LaMnO_3/SrIrO_3$ superlattices on THE from a chiral spin texture. By additively engineering the interfacial inversion symmetry with atomic-scale precision, we directly link the competition between interfacial collinear ferromagnetic interactions and DMIs to an enhanced THE. The ability to control the DMI and resulting THE points to a pathway for harnessing interfacial structures to maximize the density of chiral spin textures useful for developing high-density information storage and quantum magnets for quantum information science.

INTRODUCTION

Magnetic chirality is fundamentally linked to broken inversion symmetry, but it is rarely found in nature because only a few bulk materials have crystal structures that violate this symmetry (*1*, *2*). By contrast, inversion symmetry can be readily broken at interfaces within epitaxial heterostructures and superlattices. Moreover, inversion symmetry breaking combined with strong spin-orbit coupling (SOC) can lead to a large chiral Dzyaloshinskii-Moriya interaction (DMI), $H_{DMI} = \boldsymbol{D}_{ij} \cdot (\boldsymbol{S}_i \times \boldsymbol{S}_j)$, which imparts a handedness to the magnetic exchange interaction between adjacent spins $\boldsymbol{S}_i$ and $\boldsymbol{S}_j$ with the strength and direction expressed by the DMI vector $\boldsymbol{D}_{ij}$ (*3*, *4*). At a thin-film interface, $\boldsymbol{D}_{ij}$ lies in the plane and drives the formation of chiral Néel-type domain walls (*5*) or spin textures like the magnetic skyrmion, as depicted in Fig. 1 (A and B) (*6*). Furthermore, the Berry phase associated with the interaction between charge carriers and a chiral spin texture i.e., with scalar spin chirality $\chi_{ijk} = \boldsymbol{S}_i \cdot \boldsymbol{S}_j \times \boldsymbol{S}_k$ gives rise to an emergent magnetic field and topological Hall effect (THE) (*7*, *8*) that links the local magnetic spin texture to an electrical response. Altogether, these effects are promising phenomena that must be understood for future devices based on the electrical detection and manipulation of magnetic information (*7*, *9*–*19*).

The discovery that DMI can be tuned using different material combinations, structures, and film architectures has led to an explosion of interest in the study of thin films with 3*d* ferromagnet and heavy (i.e., 4*d* and 5*d*) element layers. In all-metal multilayers, skyrmion phases were observed within a range of temperatures and applied fields that extended well beyond the narrow phase stability regions that were first found in bulk noncentrosymmetric systems (*2*, *5*, *14*, *15*, *18*, *20*–*22*). Most recently, magnetic superlattices and multilayers with cooperative DMI from multiple interfaces enabled the study of current-induced skyrmion motion and stability up to room temperature (*14*, *15*, *23*, *24*). Despite remarkable recent advancements, it also remains a challenge to control chiral magnetic interactions to meet the size and stability requirements of spin textures for practical applications in high-density memory devices, and there is a lack of understanding of the connection between electronic transport phenomena and chiral magnetism (*7*, *11*, *19*, *25*).

Recently, it was found that the addition of oxide layers into metal multilayers could strongly enhance the strength of DMIs through interfacial electrostatics and charge transfer (*26*), while strong electronic correlations could enable exceptionally large THEs in oxide thin films (*27*). In particular, owing to the large SOC of the 5*d* element Ir and the layer-by-layer stacking and atomic control of growth achievable in epitaxial oxides, $SrIrO_3$-based heterostructures provide an excellent avenue to study the origin of interfacial DMI and the associated Hall response (*28*–*31*).

Here, we show the emergence of a highly robust chiral magnetic phase exhibiting a large THE in $LaMnO_3/SrIrO_3$ superlattices. By controlling the film architecture and interface structures, we determine that the THE originates from DMI created at the 3*d*-5*d* interface. A key observation is our ability to modulate the THE by nearly an order of magnitude through engineering of the interface symmetry with the nonmagnetic A-site layers. We discuss the relationship between THE and the role of atomic interface structure to drive the competition between interfacial collinear ferromagnetic (FM) interactions and chiral DMI as a strategy to miniaturize chiral spin textures emerging from interfaces.

[1]Materials Science and Technology Division, Oak Ridge National Laboratory, Oak Ridge, TN 37831, USA. [2]Advanced Light Source, Lawrence Berkeley National Laboratory, Berkeley, CA 94720, USA. [3]National High Field Magnet Laboratory, Florida State University, Tallahassee, FL 32310, USA. [4]Neutron Scattering Division, Oak Ridge National Laboratory, Oak Ridge, TN 37831, USA. [5]Advanced Photon Source, Argonne National Laboratory, Argonne, IL 60439, USA.
*These authors contributed equally to this work.
†Present address: Department of Physics and Astronomy, University of Arkansas at Little Rock, Little Rock, AR 72204, USA.
‡Present address: ISIS Neutron and Muon Source, STFC Rutherford Appleton Laboratory, Didcot OX11 0QX, UK.
§Corresponding author. Email: hnlee@ornl.gov

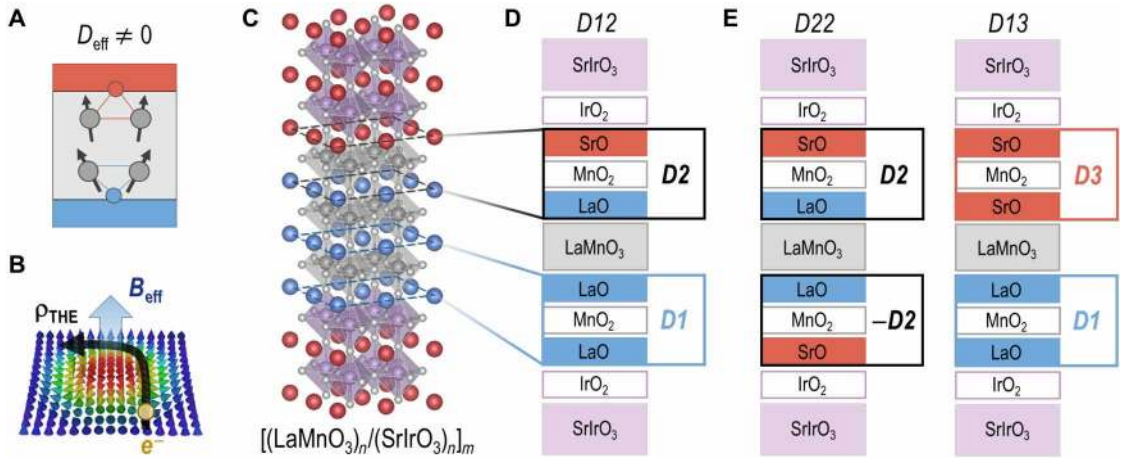

Fig. 1. Interfacial engineering of the DMI to control chiral magnetism in oxide superlattices. (**A**) A schematic illustrating an effective DMI stabilized by chiral spin textures from multiple interfaces (D_{eff}). (**B**) A schematic of the THE (ρ_{THE}) that results from the Berry phase accumulated by a charge carrier traversing a chiral spin texture. The latter acts as an emergent effective magnetic field (B_{eff}) in real space. (**C** and **D**) Control of the inversion symmetry in $LaMnO_3/SrIrO_3$ superlattices by artificially modifying the interfacial termination. Conventional growth of a superlattice with a BO_2-type layer termination creates different top and bottom interface structures (*D12*), as illustrated in (D). We simply differentiate the interface structure according to the number of connecting SrO atomic layers [i.e., *D1* indicates the stacking sequence (moving upward) LaO-MnO_2-LaO]. (**E**) DMI can be controlled within an $ABO_3/A'B'O_3$ perovskite heterostructure by engineering the interfacial layer structures by inserting SrO layers during the film growth, thus controlling inversion symmetry. Interfaces can be inversion symmetric, where the top interface is *D2* and the bottom interface is the mirror *−D2* as in superlattice *D22*, or inversion symmetry can be broken when the interface structures are different, as shown for superlattice *D13* (combining *D1* and *D3*).

RESULTS

Epitaxial $[(LaMnO_3)_n/(SrIrO_3)_n]_m$ superlattices were grown on (001) $SrTiO_3$ substrates using pulsed laser deposition (PLD). Superlattices with n = 1 to 12 unit cells (u.c.) were created with the layer repetition (m) chosen to create a total thickness of ~50 nm. X-ray diffraction scans (fig. S1) showed that all samples were phase pure and coherently strained. The natural AO-BO_2-AO-BO_2 layered structure of the perovskite ABO_3 shown in Fig. 1C (i.e., A = La or Sr, B = Mn or Ir, respectively, for $LaMnO_3$ and $SrIrO_3$) can enable systematic control over inversion symmetry of the structure by carefully tuning the layer stacking at individual interfaces. This control of the interface structure is illustrated in Fig. 1 (D and E) for three examples of $[(LaMnO_3)_n/(SrIrO_3)_n]_m$ superlattices with n and m fixed, which are either inversion symmetric or asymmetric depending on the arrangement of the interfacial A-site layers. The atomic-scale control of PLD enables each of these structures to be systematically constructed, as discussed in Materials and Methods, and verified using high-angle annular dark-field scanning transmission electron microscopy (HAADF-STEM) imaging as shown in fig. S2. This interfacial control is of central importance to identifying the competing effects between interfacial magnetic coupling and DMI.

The impact of interfacial coupling between the 3*d* and 5*d* oxide layers is reflected in the variation of field- and temperature-dependent magnetic properties with the layer thickness n (figs. S3 and S4). Compared to a single $LaMnO_3$ layer that is FM when grown using PLD (*32*), $LaMnO_3/SrIrO_3$ superlattices with n = 1 to 3 u.c. had a lower Curie temperature (T_C) and saturation magnetization (M_S) and a larger magnetic coercivity (H_C). We found a nonmonotonic relationship between M_S and n, with the largest M_S observed when n = 5. This result is consistent with the overall magnetization depending on bulk and interface magnetizations with contributions from Ir and Mn, as observed in other manganite/iridate systems (*30*, *33*, *34*) (see further consideration of the interface magnetism in Discussion). Furthermore, interfacial octahedral rotations influence the B-O-B bond angle, and interfacial charge transfer and redistribution alter the orbital occupancy, both of which modify the interfacial exchange interactions and magnetization in perovskite heterostructures (*35*–*37*). These phenomena, which act typically on short (0.4 to 2 nm) length scales (*35*), may account for the nonmonotonic relationship between layer thickness and M_S in $LaMnO_3/SrIrO_3$, as has been observed for other manganite superlattices (*38*). An increase in T_C with increasing n up to ~150 K and a decrease in H_C were observed for n = 5 to 12 u.c. All films had an easy-plane magnetic anisotropy. However, the difference in H_C measured for H applied in-plane and out-of-plane was sizeable only for $n \leq 3$ u.c. (fig. S4C). The large H_C enhancement for $n \leq 3$ u.c. resembles that of $SrMnO_3/SrIrO_3$ and $La_xSr_{1-x}MnO_3/SrIrO_3$ superlattices with magnetism dominated by charge transfer–driven interfacial collinear FM interactions (*30*, *33*). By contrast, the magnetism of superlattices with large $LaMnO_3$ thicknesses (n = 12 u.c.) was similar to that of single $LaMnO_3$ layers. Thus, the overall dependence on layer thickness suggests a competition between the interfacial interactions and intrinsic ferromagnetism of $LaMnO_3$.

To understand the influence of the interface-induced emergent magnetism on electronic transport, we measured the Hall resistivity (ρ_{xy}) as a function of H at 10 K, which is well below T_C for all superlattices. The Hall resistivity of a typical collinear ferromagnet is described by the relationship $\rho_{xy} = \rho_{OHE} + \rho_{AHE} = R_0H + R_SM$, where the ordinary ($\rho_{OHE}$) and anomalous ($\rho_{AHE}$) Hall resistivities are linear responses of the applied field (H) and magnetization (M), with respective scale factors R_0 and R_S (*8*). As shown in Fig. 2A, for short- or long-period superlattices (i.e., n = 3 and 12 u.c., respectively), the Hall resistivity is satisfactorily described by the combination of an ordinary Hall effect (OHE) and anomalous Hall effect (AHE), indicating a collinear FM state. For example, the Hall effect of n = 3 is similar to that of $SrMnO_3/SrIrO_3$ superlattices that are dominated

by collinear interfacial FM interactions (*30*). This result is also consistent with the known minimum critical thickness rule for the heavy layer, below which any DMI may be too weak to establish chiral domain walls (*39*). Furthermore, the FM state becomes energetically favorable even in the presence of DMI when the magnetic anisotropy is large (*40*), consistent with FM coinciding with an H_C enhancement for $n \leq 3$ $LaMnO_3/SrIrO_3$ superlattices. For long-period superlattices (i.e., $n = 12$ u.c.), the AHE due to ferromagnetism can be understood as a dominating effect of the intrinsic ferromagnetism of the thick layer over a diminishing (i.e., volume averaged) effect of interfacial DMI (*41*).

For intermediate $n = 4$ to 6 u.c. superlattices, however, a strongly enhanced Hall response with a dramatically different behavior emerges. In particular, a large nonmonotonic dependence on the magnetic field and a clear hysteretic behavior were observed in magnetic fields as large as 9 T, the maximum magnetic field used in Fig. 2A. Whereas the magnetization saturates for $H > 2$ T (Fig. 2B and fig. S3), the hysteresis observed in the Hall resistivity does not follow the net M or H. We noted that while multiple decoupled FM layers with opposite signs of AHE may induce field-dependent anomalies in the Hall resistivity (*42*, *43*), we observed no features in the magnetization that indicate the distinct formation of two FM layers in $LaMnO_3/SrIrO_3$. This additional Hall component for $n = 4$ to 6 u.c. superlattices can be attributed to a chiral magnetic phase induced by interfacial DMI leading to a THE (discussed in further detail below) (*1*, *7*). This is described by an additional term, ρ_{THE}, in the Hall effect (i.e., $\rho_{xy} = \rho_{OHE} + \rho_{AHE} + \rho_{THE}$). To understand the origin of the chiral magnetism and its relationship to the observed THE, we further investigated the temperature-dependent Hall effect with the $n = 5$ u.c. superlattice in magnetic fields up to 30 T. At $T = 300$ K, well above T_C, a clear linear response was observed, as shown in Fig. 2C, which is indicative of the OHE with n-type behavior. For temperatures below $T_C \sim 150$ K, an AHE due to collinear FM develops with R_S similar in magnitude to the short-period $n = 3$ u.c. superlattice. Below 50 K, the strong enhancement in ρ_{xy} was observed as a pronounced curvature, followed by the onset of hysteresis in large H.

The THE was isolated from ρ_{OHE} and ρ_{AHE} using the standard approach. The OHE was taken to be the slope of ρ_{xy} at 30 T, and the AHE was determined by extrapolating the measured magnetization to 30 T to intersect the linear H region of ρ_{xy}, as shown in Fig. 2D. The resulting THE is shown as a function of T and H in Fig. 2E, which was measured on sweeping H from +30 to −30 T. The circles and dotted line provide an estimate of the phase stability region with $|\rho_{xy}| < 1$ μΩ·cm, which is wide compared to previous reports for systems with interfacial DMI. The maximum THE at each temperature shown in Fig. 2F is quite large compared to layered oxides or bulk materials with strong DMI that are typically on the order of a few nΩ·cm to 1 μΩ·cm. Recent theoretical investigations have also identified the possibility of strong DMI and THE originating at the iridate/manganite interface, consistent with our experimental observations [see fig. S5, section S2, and (*44*)]. These results point to a highly robust chiral phase stabilized in the intermediate-period $LaMnO_3/SrIrO_3$ superlattices with $n = 4$ to 6 u.c.

The relationships among inversion symmetry, DMI, and the THE were further tested by examining $n = 5$ u.c. superlattices grown with the different interface layer structures *D12*, *D22*, and *D13* that are shown schematically in Fig. 1 (D and E). The hypothesis is that the extent of inversion symmetry breaking with respect to the $LaMnO_3$ layer should be reflected in the strength of the total DMI that is created additively from multiple interfaces in the superlattice. Because of the THE results from the interaction between charge carriers and a spatially varying magnetic spin texture, the magnitude of the THE depends on the winding number and density of the chiral spin features that establish the total topological charge (n_t) of the system (*7*, *8*). For Néel-type skyrmions, in the adiabatic limit of the Berry phase description, ρ_{THE} is proportional to the skyrmion density, $n_{sk} = n_t$, and inversely proportional to the skyrmion size, $D_{sk} \sim n_{sk}^{-1/2}$, for a close packed arrangement of the spin texture (*2*, *20*, *45*). Note that the skyrmion density and thus THE is determined by the competition between DMI, FM exchange, and magnetic anisotropy energy terms governing the magnetic system. For our $LaMnO_3/SrIrO_3$ superlattices with different A-site layer structures,

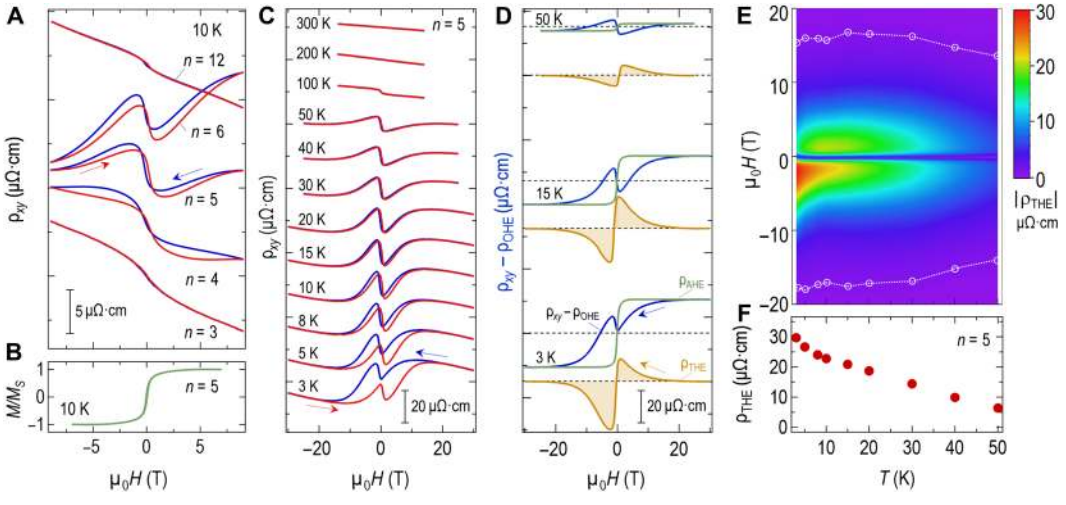

Fig. 2. The Hall effect in LaMnO3/SrIrO3 superlattices. (**A**) The Hall effect ρ_{xy} measured at 10 K and shown for superlattices $n = 3$ to 12 u.c. *D12*-type superlattices. (**B**) The magnetization measured for the $n = 5$ u.c. superlattice, which is similar for all n on the scale shown. (**C**) Temperature dependence of the Hall resistivity (ρ_{xy}) for the $n = 5$ u.c. superlattice measured in fields up to 30 T. (**D**) Determination of the topological Hall resistivity ρ_{THE} of $n = 5$ u.c. at several temperatures obtained for the decreasing (+H to −H) applied magnetic field measurements. (**E**) The topological Hall resistivity (ρ_{THE}) shown as functions of temperature and applied field. (**F**) Temperature dependence of the maximum value of ρ_{THE} taken from (D) and (E). Data in (A) to (D) are shown with a vertical offset for clarity.

the Hall effect is shown in Fig. 3 (A and B). We observe that the amplitude of ρ_{THE} measured at T = 10 K for *D13* is ~75 μΩ·cm, which is near an order of magnitude larger than *D22* and a factor of 3 larger than *D12*. The enhanced THE is independent of the conventional magnetic properties (e.g., T_C, H_C, or M_S), which is consistent with the THE being directly linked to the interface structure and DMI. We note that the global inversion symmetry breaking due to the surface and substrate are unavoidable and that other magnetic interactions existing in the superlattice (e.g., dipolar interactions) may help to stabilize chiral structures even with weakened DMI that may contribute to a persistent THE in even the most symmetric superlattice structure. Relative to the naturally occurring superlattice *D12*, we attribute the suppressed ρ_{THE} of *D22* to the symmetric interface structure creating a weakened total DMI, and we attribute the large enhancement of ρ_{THE} in *D13* to the largest total DMI from fully different top and bottom interface layer structures.

Because the enhanced Hall effect created by the controlled film architecture and interface structures of our 3*d*-5*d* system is consistent with effects of interfacial DMI, we consider the relationship between DMI, THE, and real-space spin texture. In thin films, the interface geometry necessarily sets the spin rotation direction induced by DMI to favor chiral Néel-type domain walls (*5*). For this reason, although we do not have a direct image of a chiral spin texture in $LaMnO_3/SrIrO_3$, we propose that the $LaMnO_3/SrIrO_3$ system may host Néel-type skyrmions or chiral domain walls, while we strongly believe that our observation of the THE indicates the potential formation of skyrmions (see the Supplementary Materials for more details on skyrmion confirmation). Although establishing a quantitative description of skyrmion textures directly from Hall effects remains a challenge for complex systems with multiple magnetic layers, conduction pathways, or possible nonadiabatic effects (*7*, *8*, *18*, *25*, *27*, *46*, *47*), a qualitative proportionality between the magnitude of the THE and n_t appears robust (*7*, *20*, *47*). Consequently, an increase in ρ_{THE} signifies a denser array of chiral features and hence a smaller feature size, even when the absolute feature size is difficult to establish. Thus, we illustrate the impact of different interfacial A-site layer structures of the n = 5 u.c. $LaMnO_3/SrIrO_3$ superlattice to a possible relative change in chiral spin feature density $\Delta n_t = \rho_{THE}/[\rho_{THE}(D22)]$ and feature size ($\Delta n_t^{-1/2}$) in Fig. 3 (B and C) (*7*) (section S2). This indicates that engineering the nonmagnetic interfacial atomic layers is an effective strategy for tuning the chiral interactions and inversion symmetry to ultimately shrink the size of chiral spin textures originating from interfaces. From the topological Hall resistivity, we estimate that the size of potential skyrmions can be as small as 2 nm (see section S2 for further details).

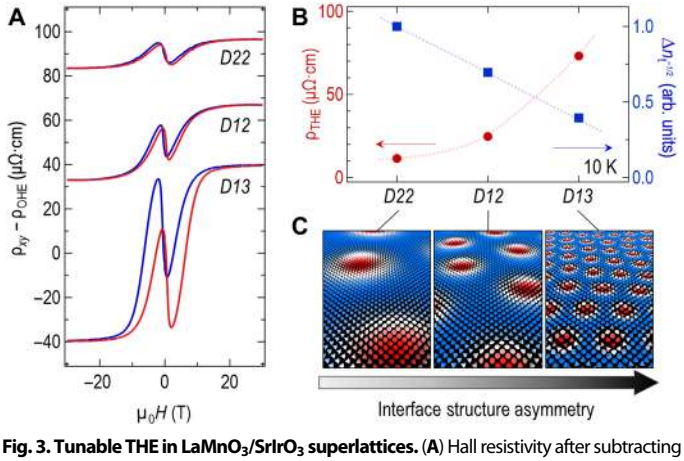

Fig. 3. Tunable THE in $LaMnO_3/SrIrO_3$ superlattices. (**A**) Hall resistivity after subtracting the OHE measured at 10 K for n = 5 u.c. superlattices with interface types *D22*, *D12*, and *D13* shown in Fig. 1D. (**B**) The maximum value of (left axis) ρ_{THE} and (right axis) relative spin feature size ($\Delta n_t^{-1/2}$) measured at 10 K. (**C**) An illustration of the relative change in density of topological charges (n_t) obtained from the observed variation in ρ_{THE} that demonstrates a miniaturization of the spin feature size ($\Delta n_t^{-1/2}$) by tuning the interfacial magnetic interactions using highly inversion-asymmetric interfacial structures.

To gain deeper insight into the magnetic interaction energy terms that govern magnetic domain formation in $LaMnO_3/SrIrO_3$ superlattices, we examined the temperature dependence of the spontaneous (i.e., zero field) domain structure using photoemission electron microscopy (PEEM) combined with Mn L_3-edge x-ray magnetic circular dichroism (XMCD). Because of the grazing incidence geometry of the incoming x-rays, XMCD-PEEM provides a spatial map of the dominant in-plane projection of the Mn magnetization. Images of an n = 5 u.c. superlattice measured while cooling from 100 to 32 K are shown in Fig. 4A. These images reveal a dense domain structure formed at temperatures near the onset T ~ 90 K of the THE. The $LaMnO_3/SrIrO_3$ superlattice showed essentially no fluctuations in shape or domain coalescence upon decreasing temperature; this contrasts with the typical behavior of collinear FM phases (see section S4 and fig. S6 for further analysis and interpretation of PEEM images). This result suggests a highly energetically favorable domain structure formed in $LaMnO_3/SrIrO_3$ that is strongly affected by an energy term that is not typical of FM systems but that is consistent with strong DMI.

Because XMCD-PEEM allows the direct imaging of nanoscale magnetic features, it is well suited to identify chiral domain wall and skyrmion textures (*16*). To examine the impact of DMI on the domain structure in $LaMnO_3/SrIrO_3$ superlattices, we performed micromagnetic simulations of the spontaneous domain structure of a simple manganite layer with interfacial DMI using Object Oriented Micromagnetic Framework (*48*). We found that the structures observed with XMCD-PEEM closely resemble the mixed stripe and bubble features that can evolve into a skyrmion phase in a sizable applied magnetic field and which are only observed when a DMI term is included in the magnetic simulation parameters (see section S3 and figs. S5 to S7 for detailed comparison of XMCD-PEEM images and micromagnetic simulations).

To examine the element-specific electronic and magnetic details to understand the origin of the magnetism of the $LaMnO_3/SrIrO_3$ system, we conducted x-ray absorption spectroscopy (XAS) and XMCD measurements of Mn and Ir L-edges of n = 5 u.c. $LaMnO_3/SrIrO_3$ superlattice, as shown in Fig. 4 (B and C). The magnetism originates predominantly from the $LaMnO_3$ layer, as revealed by a large Mn XMCD signal, consistent with FM $LaMnO_3$ films grown by PLD (*32*). We observed null L_3-edge and weak L_2-edge Ir XMCD signal that indicates a small Ir magnetization in the n = 5 u.c. $LaMnO_3/SrIrO_3$ superlattice. By comparison, the Ir and Mn XMCD of short-period $SrMnO_3/SrIrO_3$ and $La_{2/3}Sr_{1/3}MnO_3/SrIrO_3$ superlattices with strong interfacial FM interactions showed clear XMCD at both the L_3- and L_2-edges (*30*, *33*), indicating a much larger Ir magnetization in those systems. Our lack of observed L_3-edge XMCD indicates change in the element-specific magnetism, with a possible canting of the Ir moment away from the applied field direction for the n = 5 $LaMnO_3/SrIrO_3$ superlattice, compared to previously studied FM iridate/manganite systems. These observations are

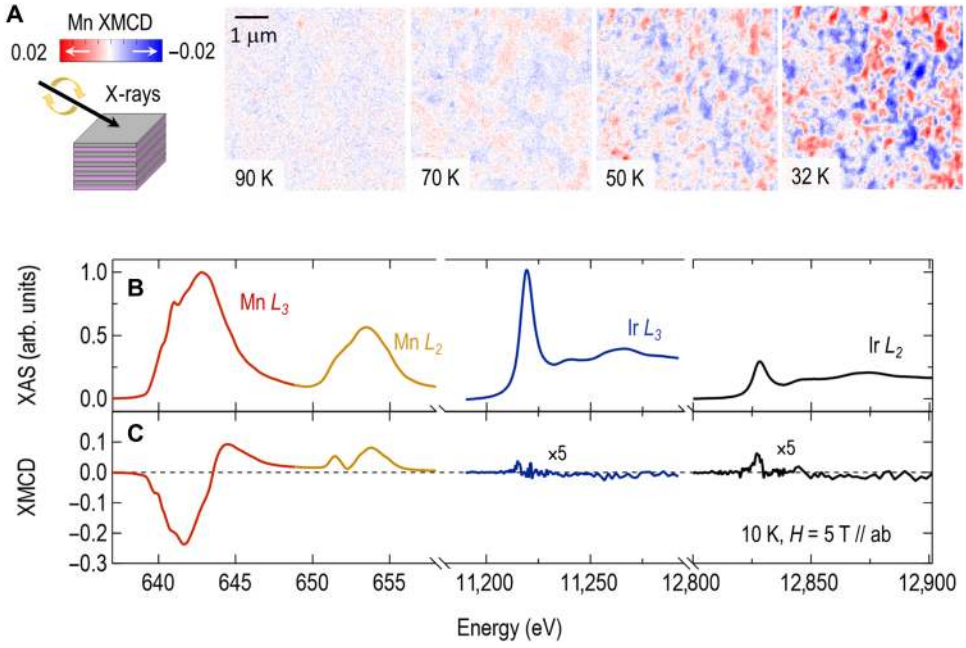

Fig. 4. Domain structure and element-specific magnetism of a $LaMnO_3/SrIrO_3$ superlattice. (**A**) XMCD-PEEM images at various temperatures for an $n = 5$ u.c. *D12* superlattice and (**B**) XAS and (**C**) XMCD measured at 10 K and 5 T for the Mn and Ir *L*-edges for $n = 5$ u.c.

consistent with the Ir-Mn interfacial coupling modified by weakened collinear interfacial interactions and strong DMI in the $n = 5$ u.c. $LaMnO_3/SrIrO_3$ superlattice versus a predominance of strong collinear interfacial exchange interactions in short-period ($n = 1$ to 3 u.c.) superlattices that qualitatively agrees with the layer thickness–dependent onset of THE in $LaMnO_3/SrIrO_3$ superlattices.

DISCUSSION

Because the DMI is determined by magnetic interactions within a single atomic layer of the interface, local interface structures are expected to have a critical role in the emergence of THEs. To understand the mechanism responsible for the THE of $LaMnO_3/SrIrO_3$ superlattices, we consider the importance of interfacial chemistry and symmetry that drive the Mn valence and exchange interactions that govern the magnetism of artificially engineered manganite superlattices (*36*, *37*). Specifically, because of charge leakage that is effective over 1 to 2 u.c., short-period ($n \leq 3$ u.c.) $[(LaMnO_3)_{2n}/(SrMnO_3)_n]$ superlattices display double exchange–driven ferromagnetism and conductivity that are similar to those of the $La_{0.66}Sr_{0.33}MnO_3$ alloy instead of insulating antiferromagnetism intrinsic to the constituent materials. We propose that the presence of both interfacial LaO and SrO layers can promote a mixed Mn valence and a similar charge leakage in short-period $LaMnO_3/SrIrO_3$ superlattices. This phenomenon can lead to a strengthened interfacial FM double exchange that directly competes with DMI and thus result in the appearance of an AHE due to an FM ground state in our $n \leq 3$ u.c. $LaMnO_3/SrIrO_3$ superlattices. This behavior is in agreement with conventional understanding that the stabilization of chiral phases depends critically on the competition between DMI, collinear FM interactions, and magnetic anisotropy of a system (*19*, *39*, *40*). It is also likely that the distinct local Mn environment and magnetism at the polar-nonpolar interface bridged by LaO and SrO layers differ from the uniform LaO-MnO_2-LaO environment of the bulk. This difference in interface and bulk environments likely contributes to the strong influence of interface versus intrinsic properties in the intermediate n systems, such as nonmonotonic n and THE dependence. Furthermore, our ability to modulate the magnitude of the THE for the $n = 5$ u.c. superlattice reveals that control of the interface structure driven by interfacial A-site layers can be a highly effective method for tuning DMI.

In summary, the interfacial inversion symmetry of 3*d*-5*d* $LaMnO_3/SrIrO_3$ superlattices is deliberately controlled to modify the competition between chiral DMI and intrinsic collinear ferromagnetism. This interfacial symmetry control led to a large THE, which originates from a highly robust chiral magnetic phase, potentially hosting skyrmions. Our findings shed light on development of novel pathways to stabilize ultrahigh-density chiral spin textures important for developing topologically protected quantum magnets.

MATERIALS AND METHODS

Sample synthesis and structural characterization

All samples were synthesized by pulsed laser epitaxy with a substrate temperature, oxygen partial pressure, and laser fluence of 700°C, 100 mTorr, and 1.0 J/cm^2, respectively, on atomically flat TiO_2-terminated (001) $SrTiO_3$ substrates with a KrF eximer laser ($\lambda = 248$ nm). The crystal structure, phase purity, and orientation of these films and superlattices were confirmed by x-ray reflectivity and diffraction measurements using a four-circle x-ray diffractometer. Superlattices with $n = 1$ to 12 u.c. thick layers were prepared using a typical two-target growth alternating $LaMnO_3$ and $SrIrO_3$ to produce the structure type *D12*. For superlattices with $n = 5$ u.c., two additional superlattice structures were created by controlling the interface growth by replacing either the bottom or top 1 u.c. of $LaMnO_3$ with $SrMnO_3$; this resulted in the structures *D22* or *D13*, respectively.

HAADF-STEM imaging was carried out in Nion UltraSTEM200 operated at 200 kV. The microscope is equipped with a cold field-emission gun and an aberration corrector for subangstrom resolution.

An inner angle of 78 mrad was used for HAADF imaging. The convergence semiangle for the electron probe was set to 30 mrad.

Physical properties characterization

The magnetization was determined with a 7 T Quantum Design MPMS3, measured using conventional techniques from hysteresis loop measurements at 10 K and up to 7 T, after subtracting a linear background to correct for the diamagnetic response of the $SrTiO_3$ substrate. The electronic transport measurements were performed with a 14 T Quantum Design Physical Property Measurement System with custom electronics. The electrical contacts were made by ultrasonic soldering Au wires with In solder in a van der Pauw configuration. Magnetotransport properties of thin films under high magnetic field up to 30 T were measured at the National High Magnetic Field Laboratory (NHMFL) in Tallahassee.

X-ray absorption experiments

X-ray absorption, magnetic circular dichroism, and linear dichroism were measured at the Advanced Photon Source at Argonne National Laboratory at beamlines 4-ID-C and 4-ID-D. Measurements of Mn $L_{2,3}$-edge were done in total electron yield and fluorescence yield modes at a grazing angle to the sample surface. The XMCD at 10 K was obtained from the average of ±5 T magnetic fields applied in the film plane to correct for possible nonmagnetic artifacts. All spectra were normalized to a maximum XAS intensity at the L_3-edge to facilitate direct comparison between the Ir and Mn L-edges. Variable-temperature XMCD-PEEM images were measured at the Advanced Light Source at Lawrence Berkeley National Laboratory at sector 11.0.1 using the PEEM-3 endstation. Images were collected on films grown on a conducting Nb-doped (0.05%) $SrTiO_3$ substrate and were measured using the Mn L_3-edge XMCD in zero applied magnetic field at a grazing angle of 30% to the film surface, which provides a predominant (86.6%) contrast for the in-plane magnetization versus 50% for the out-of-plane magnetization.

SUPPLEMENTARY MATERIALS

Supplementary material for this article is available at http://advances.sciencemag.org/cgi/content/full/6/27/eaaz3902/DC1

REFERENCES AND NOTES

1. K. Ohgushi, S. Murakami, N. Nagaosa, Spin anisotropy and quantum Hall effect in the *kagomé* lattice: Chiral spin state based on a ferromagnet. *Phys. Rev. B* **62**, R6065 (2000).
2. S. Mühlbauer, B. Binz, F. Jonietz, C. Pfleiderer, A. Rosch, A. Neubauer, R. Georgii, P. Boni, Skyrmion lattice in a chiral magnet. *Science* **323**, 915–919 (2009).
3. I. Dzyaloshinsky, A thermodynamic theory of "weak" ferromagnetism of antiferromagnetics. *J. Phys. Chem. Solid* **4**, 241–255 (1958).
4. T. Moriya, Anisotropic superexchange interaction and weak ferromagnetism. *Phys. Rev.* **120**, 91 (1960).
5. M. Bode, M. Heide, K. von Bergmann, P. Ferriani, S. Heinze, G. Bihlmayer, A. Kubetzka, O. Pietzsch, S. Blügel, R. Wiesendanger, Chiral magnetic order at surfaces driven by inversion asymmetry. *Nature* **447**, 190–193 (2007).
6. U. K. Rößler, A. N. Bogdanov, C. Pfleiderer, Spontaneous skyrmion ground states in magnetic metals. *Nature* **442**, 797–801 (2006).
7. P. Bruno, V. K. Dugaev, M. Taillefumier, Topological Hall effect and Berry phase in magnetic nanostructures. *Phys. Rev. Lett.* **93**, 096806 (2004).
8. N. Nagaosa, J. Sinova, S. Onoda, A. H. MacDonald, N. P. Ong, Anomalous Hall effect. *Rev. Mod. Phys.* **82**, 1539 (2010).
9. A. N. Bogdanov, U. K. Rößler, Chiral symmetry breaking in magnetic thin films and multilayers. *Phys. Rev. Lett.* **87**, 037203 (2001).
10. S. S. Parkin, M. Hayashi, L. Thomas, Magnetic domain-wall racetrack memory. *Science* **320**, 190 (2008).
11. N. Nagaosa, Y. Tokura, Topological properties and dynamics of magnetic skyrmions. *Nat. Nanotechnol.* **8**, 899–911 (2013).
12. P. Milde, D. Köhler, J. Seidel, L. M. Eng, A. Bauer, A. Chacon, J. Kindervater, S. Mühlbauer, C. Pfleiderer, S. Buhrandt, C. Schütte, A. Rosch, Unwinding of a skyrmion lattice by magnetic monopoles. *Science* **340**, 1076–1080 (2013).
13. W. Jiang, P. Upadhyaya, W. Zhang, G. Yu, M. B. Jungfleisch, F. Y. Fradin, J. E. Pearson, Y. Tserkovnyak, K. L. Wang, O. Heinonen, S. G. te Velthuis, A. Hoffmann, Blowing magnetic skyrmion bubbles. *Science* **349**, 283–286 (2015).
14. C. Moreau-Luchaire, S. C. Mouta, N. Reyren, J. Sampaio, C. A. Vaz, N. Van Horne, K. Bouzehouane, K. Garcia, C. Deranlot, P. Warnicke, P. Wohlhüter, J.-M. George, M. Weigand, J. Raabe, V. Cros, A. Fert, Additive interfacial chiral interaction in multilayers for stabilization of small individual skyrmions at room temperature. *Nat. Nanotechnol.* **11**, 444–448 (2016).
15. S. Woo, K. Litzius, B. Krüger, M.-Y. Im, L. Caretta, K. Richter, M. Mann, A. Krone, R. M. Reeve, M. Weigand, P. Agrawal, I. Lemesh, M.-A. Mawass, P. Fischer, M. Kläui, G. S. Beach, Observation of room-temperature magnetic skyrmions and their current-driven dynamics in ultrathin metallic ferromagnets. *Nat. Mater.* **15**, 501–506 (2016).
16. O. Boulle, J. Vogel, H. Yang, S. Pizzini, D. de Souza Chaves, A. Locatelli, T. O. Menteş, A. Sala, L. D. Buda-Prejbeanu, O. Klein, M. Belmeguenai, Y. Roussigné, A. Stashkevich, S. M. Chérif, L. Aballe, M. Foerster, M. Chshiev, S. Auffret, I. M. Miron, G. Gaudin, Room-temperature chiral magnetic skyrmions in ultrathin magnetic nanostructures. *Nat. Nanotechnol.* **11**, 449–454 (2016).
17. G. Yu, P. Upadhyaya, X. Li, W. Li, S. K. Kim, Y. Fan, K. L. Wong, Y. Tserkovnyak, P. K. Amiri, K. L. Wang, Room-temperature creation and spin–orbit torque manipulation of skyrmions in thin films with engineered asymmetry. *Nano Lett.* **16**, 1981–1988 (2016).
18. A. Soumyanarayanan, M. Raju, A. L. Gonzalez Oyarce, A. K. C. Tan, M.-Y. Im, A. P. Petrović, P. Ho, K. H. Khoo, M. Tran, C. K. Gan, F. Ernult, C. Panagopoulos, Tunable room-temperature magnetic skyrmions in Ir/Fe/Co/Pt multilayers. *Nat. Mater.* **16**, 898–904 (2017).
19. A. Fert, N. Reyren, V. Cros, Magnetic skyrmions: Advances in physics and potential applications. *Nat. Revs. Mater.* **2**, 17031 (2017).
20. A. Neubauer, C. Pfleiderer, B. Binz, A. Rosch, R. Ritz, P. G. Niklowitz, P. Böni, Topological Hall effect in the A phase of MnSi. *Phys. Rev. Lett.* **102**, 186602 (2009).
21. S. Heinze, K. von Bergmann, M. Menzel, J. Brede, A. Kubetzka, R. Wiesendanger, G. Bihlmayer, S. Blügel, Spontaneous atomic-scale magnetic skyrmion lattice in two dimensions. *Nat. Phys.* **7**, 713–718 (2011).
22. S. Seki, X. Z. Yu, S. Ishiwata, Y. Tokura, Observation of skyrmions in a multiferroic material. *Science* **336**, 198–201 (2012).
23. N. Romming, C. Hanneken, M. Menzel, J. E. Bickel, B. Wolter, K. von Bergmann, A. Kubetzka, R. Wiesendanger, Writing and deleting single magnetic skyrmions. *Science* **341**, 636–639 (2013).
24. L. Caretta, M. Mann, F. Büttner, K. Ueda, B. Pfau, C. M. Günther, P. Hessing, A. Churikova, C. Klose, M. Schneider, D. Engel, C. Marcus, D. Bono, K. Bagschik, S. Eisebitt, G. S. D. Beach, Fast current-driven domain walls and small skyrmions in a compensated ferrimagnet. *Nat. Nanotechnol.* **13**, 1154–1160 (2018).
25. H. Ishizuka, N. Nagaosa, Spin chirality induced skew scattering and anomalous Hall effect in chiral magnets. *Sci. Adv.* **4**, eaap9962 (2018).
26. A. Belabbes, G. Bihlmayer, S. Blügel, A. Manchon, Oxygen-enabled control of Dzyaloshinskii-Moriya Interaction in ultra-thin magnetic films. *Sci. Rep.* **6**, 24634 (2016).
27. L. Vistoli, W. Wang, A. Sander, Q. Zhu, B. Casals, R. Cichelero, A. Barthélémy, S. Fusil, G. Herranz, S. Valencia, R. Abrudan, E. Weschke, K. Nakazawa, H. Kohno, J. Santamaria, W. Wu, V. Garcia, M. Bibes, Giant topological Hall effect in correlated oxide thin films. *Nat. Phys.* **15**, 67–72 (2018).
28. H. Y. Hwang, Y. Iwasa, M. Kawasaki, B. Keimer, N. Nagaosa, Y. Tokura, Emergent phenomena at oxide interfaces. *Nat. Mater.* **11**, 103–113 (2012).
29. J. Matsuno, N. Ogawa, K. Yasuda, F. Kagawa, W. Koshibae, N. Nagaosa, Y. Tokura, M. Kawasaki, Interface-driven topological Hall effect in $SrRuO_3$-$SrIrO_3$ bilayer. *Sci. Adv.* **2**, e1600304 (2016).
30. J. Nichols, X. Gao, S. Lee, T. L. Meyer, J. W. Freeland, V. Lauter, D. Yi, J. Liu, D. Haskel, J. R. Petrie, E.-J. Guo, A. Herklotz, D. Lee, T. Z. Ward, G. Eres, M. R. Fitzsimmons, H. N. Lee, Emerging magnetism and anomalous Hall effect in iridate-manganite heterostructures. *Nat. Commun.* **7**, 12721 (2016).
31. Y. Li, L. Zhang, Q. Zhang, C. Li, T. Yang, Y. Deng, L. Gu, D. Wu, Emergent topological Hall effect in $La_{0.7}Sr_{0.3}MnO_3$/$SrIrO_3$ heterostructures. *ACS Appl. Mater. Inter.* **11**, 21268–21274 (2019).
32. W. S. Choi, Z. Marton, S. Y. Jang, S. J. Moon, B. C. Jeon, J. H. Shin, S. S. A. Seo, T. W. Noh, K. Myung-Whun, H. N. Lee, Y. S. Lee, Effects of oxygen-reducing atmosphere annealing on $LaMnO_3$ epitaxial thin films. *J. Phys. D Appl. Phys.* **42**, 165401 (2009).
33. D. Yi, J. Liu, S.-L. Hsu, L. Zhang, Y. Choi, J.-W. Kim, Z. Chen, J. D. Clarkson, C. R. Serrao, E. Arenholz, P. J. Ryan, H. Xu, R. J. Birgeneau, R. Ramesh, Atomic-scale control of magnetic anisotropy via novel spin-orbit coupling effect in $La_{2/3}Sr_{1/3}MnO_3$/$SrIrO_3$ superlattices. *Proc. Natl. Acad. Sci. U.S.A.* **113**, 6397–6402 (2016).
34. S. Okamoto, J. Nichols, C. Sohn, S. Y. Kim, T. W. Noh, H. N. Lee, Charge transfer in iridate-manganite superlattices. *Nano Lett.* **17**, 2126–2130 (2017).

35. F. Hellman, A. Hoffmann, Y. Tserkovnyak, G. S. D. Beach, E. E. Fullerton, C. Leighton, A. H. MacDonald, D. C. Ralph, D. A. Arena, H. A. Dürr, P. Fischer, J. Grollier, J. P. Heremans, T. Jungwirth, A. V. Kimel, B. Koopmans, I. N. Krivorotov, S. J. May, A. K. Petford-Long, J. M. Rondinelli, N. Samarth, I. K. Schuller, A. N. Slavin, M. D. Stiles, O. Tchernyshyov, A. Thiaville, B. L. Zink, Interface-induced phenomena in magnetism. *Rev. Mod. Phys.* **89**, 025006 (2017).
36. Ş. Smadici, P. Abbamonte, A. Bhattacharya, X. Zhai, B. Jiang, A. Rusydi, J. N. Eckstein, S. D. Bader, J.-M. Zuo, Electronic reconstruction at $SrMnO_3$-$LaMnO_3$ superlattice interfaces. *Phys. Rev. Lett.* **99**, 196404 (2007).
37. A. Bhattacharya, S. J. May, S. G. te Velthuis, M. Warusawithana, X. Zhai, B. Jiang, J.-M. Zuo, M. R. Fitzsimmons, S. D. Bader, J. N. Eckstein, Metal-insulator transition and its relation to magnetic structure in $(LaMnO_3)_{2n}/(SrMnO_3)_n$ superlattices. *Phys. Rev. Lett.* **100**, 257203 (2008).
38. X. Zhai, L. Cheng, Y. Liu, C. M. Schlepütz, S. Dong, H. Li, X. Zhang, S. Chu, L. Zheng, J. Zhang, A. Zhao, H. Hong, A. Bhattacharya, J. N. Eckstein, C. Zeng, Correlating interfacial octahedral rotations with magnetism in $(LaMnO_{3+\delta})_N/(SrTiO_3)_N$ superlattices. *Nat. Commun.* **5**, 4283 (2014).
39. S. Tacchi, R. E. Troncoso, M. Ahlberg, G. Gubbiotti, M. Madami, J. Åkerman, P. Landeros, Interfacial Dzyaloshinskii-Moriya interaction in Pt/CoFeB films: Effect of the heavy-metal thickness. *Phys. Rev. Lett.* **118**, 147201 (2017).
40. S. Rohart, A. Thiaville, Skyrmion confinement in ultrathin film nanostructures in the presence of Dzyaloshinskii-Moriya interaction. *Phys. Rev. B* **88**, 184422 (2013).
41. H. T. Nembach, J. M. Shaw, M. Weiler, E. Jué, T. J. Silva, Linear relation between Heisenberg exchange and interfacial Dzyaloshinskii–Moriya interaction in metal films. *Nat. Phys.* **11**, 825–829 (2015).
42. D. J. Groenendijk, C. Autieri, T. C. van Thiel, W. Brzezicki, N. Gauquelin, P. Barone, H. W. van de Bos, S. van Aert, J. Verbeeck, A. Filippetti, S. Picozzi, M. Cuoco, A. D. Caviglia, Berry Phase Engineering at Oxide Interfaces. arXiv:1810.05619 (2018).
43. D. Kan, T. Moriyama, K. Kobayashi, Y. Shimakawa, Alternative to the topological interpretation of the transverse resistivity anomalies in $SrRuO_3$. *Phys. Rev. B* **98**, 180408 (2018).
44. N. Mohanta, E. Dagotto, S. Okamoto, Topological Hall effect and emergent skyrmion crystal at manganite-iridate oxide interfaces. *Phys. Rev. B* **100**, 064429 (2019).
45. M. Lee, W. Kang, Y. Onose, Y. Tokura, N. P. Ong, Unusual Hall effect anomaly in MnSi under pressure. *Phys. Rev. Lett.* **102**, 186601 (2009).
46. D. Maccariello, W. Legrand, N. Reyren, K. Garcia, K. Bouzehouane, S. Collin, V. Cros, A. Fert, Electrical detection of single magnetic skyrmions in metallic multilayers at room temperature. *Nat. Nanotechnol.* **13**, 233–237 (2018).
47. M. Raju, A. Yagil, A. Soumyanarayanan, A. K. C. Tan, A. Almoalem, F. Ma, O. M. Auslaender, C. Panagopoulos, The evolution of skyrmions in Ir/Fe/Co/Pt multilayers and their topological Hall signature. *Nat. Commun.* **10**, 696 (2019).
48. M. J. Donahue, D. G. Porter, OOMMF User's Guide, Version 1.0, Interagency Report NISTIR 6376 (National Institute of Standards and Technology, Gaithersburg, MD, 1999).
49. L. Liu, Q. Qin, W. Lin, C. Li, Q. Xie, S. He, X. Shu, C. Zhou, Z. Lim, J. Yu, W. Lu, M. Li, X. Yan, S. J. Pennycook, J. Chen, Current-induced magnetization switching in all-oxide heterostructures. *Nat. Nanotechnol.* **14**, 939–944 (2019).
50. T. Nan, T. J. Anderson, J. Gibbons, K. Hwang, N. Campbell, H. Zhou, Y. Q. Dong, G. Y. Kim, D. F. Shao, T. R. Paudel, N. Reynolds, X. J. Wang, N. X. Sun, E. Y. Tsymbal, S. Y. Choi, M. S. Rzchowski, Y. B. Kim, D. C. Ralph, C. B. Eom, Anisotropic spin-orbit torque generation in epitaxial $SrIrO_3$ by symmetry design. *Proc. Natl. Acad. Sci. U.S.A.* **116**, 16186–16191 (2019).
51. S. J. Moon, H. Jin, K. W. Kim, W. S. Choi, Y. S. Lee, J. Yu, G. Cao, A. Sumi, H. Funakubo, C. Bernhard, T. W. Noh, Dimensionality-controlled insulator-metal transition and correlated metallic state in 5*d* transition metal oxides $Sr_{n+1}Ir_n O_{3n+1}$ (n=1, 2, and infinity). *Phys. Rev. Lett.* **101**, 226402 (2008).
52. Y. F. Nie, P. D. King, C. H. Kim, M. Uchida, H. I. Wei, B. D. Faeth, J. P. Ruf, J. P. Ruff, L. Xie, X. Pan, C. J. Fennie, D. G. Schlom, K. M. Shen, Interplay of spin-orbit interactions, dimensionality, and octahedral rotations in semimetallic $SrIrO_3$. *Phys. Rev. Lett.* **114**, 016401 (2015).
53. Z. T. Liu, M. Y. Li, Q. F. Li, J. S. Liu, W. Li, H. F. Yang, Q. Yao, C. C. Fan, X. G. Wan, Z. Wang, D. W. Shen, Direct observation of the Dirac nodes lifting in semimetallic perovskite $SrIrO_3$ thin films. *Sci. Rep.* **6**, 30309 (2016).
54. J. Matsuno, K. Ihara, S. Yamamura, H. Wadati, K. Ishii, V. V. Shankar, H.-Y. Kee, H. Takagi, Engineering a spin-orbital magnetic insulator by tailoring superlattices. *Phys. Rev. Lett.* **114**, 247209 (2015).
55. J.-H. Park, E. Vescovo, H.-J. Kim, C. Kwon, R. Ramesh, T. Venkatesan, Direct evidence for a half-metallic ferromagnet. *Nature* **392**, 794–796 (1998).
56. H. Boschker, M. Mathews, P. Brinks, E. Houwman, A. Vailionis, G. Koster, D. H. A. Blank, G. Rijnders, Uniaxial contribution to the magnetic anisotropy of $La_{0.67}Sr_{0.33}MnO_3$ thin films induced by orthorhombic crystal structure. *J. Magn. Magn. Mater.* **323**, 2632–2638 (2011).
57. V. Walter, "Interactions between lipid membranes and self-assembling cell-penetrating peptides," thesis, Institut Charles Sadron (2017).
58. J. Schindelin, I. Arganda-Carreras, E. Frise, V. Kaynig, M. Longair, T. Pietzsch, S. Preibisch, C. Rueden, S. Saalfeld, B. Schmid, J.-Y. Tinevez, D. J. White, V. Hartenstein, K. Eliceiri, P. Tomancak, A. Cardona, Fiji: An open-source platform for biological-image analysis. *Nat. Methods* **9**, 676–682 (2012).
59. C. Baldasseroni, C. Bordel, C. Antonakos, A. Scholl, K. H. Stone, J. B. Kortright, F. Hellman, Temperature-driven growth of antiferromagnetic domains in thin-film FeRh. *J. Phys. Condens. Matter* **27**, 256001 (2015).
60. R. V. Chopdekar, J. Heidler, C. Piamonteze, Y. Takamura, A. Scholl, S. Rusponi, H. Brune, L. J. Heyderman, F. Nolting, Strain-dependent magnetic configurations in manganite-titanate heterostructures probed with soft X-ray techniques. *Eur. Phys. J. B.* **86**, 241 (2013).
61. R. V. Chopdekar, M. Buzzi, C. Jenkins, E. Arenholz, F. Nolting, Y. Takamura, Giant reversible anisotropy changes at room temperature in a $(La,Sr)MnO_3/Pb(Mg,Nb,Ti)O_3$ magneto-electric heterostructure. *Sci. Rep.* **6**, 27501 (2016).
62. S. R. Bakaul, W. Lin, T. Wu, Evolution of magnetic bubble domains in manganite films. *Appl. Phys. Lett.* **99**, 042503 (2011).
63. W. T. Heller, M. Cuneo, L. Debeer-Schmitt, C. Do, L. He, L. Heroux, K. Littrell, S. V. Pingali, S. Qian, C. Stanley, V. S. Urban, B. Wu, W. Bras, The suite of small-angle neutron scattering instruments at Oak Ridge National Laboratory. *J. Appl. Cryst.* **51**, 242–248 (2018).
64. G. D. Wignall, K. C. Littrell, W. T. Heller, Y. B. Melnichenko, K. M. Bailey, G. W. Lynn, D. A. Myles, V. S. Urban, M. V. Buchanan, D. L. Selby, P. D. Butler, The 40 m general purpose small-angle neutron scattering instrument at Oak Ridge National Laboratory. *J. Appl. Cryst.* **45**, 990–998 (2012).

Acknowledgments: We thank M. R. Fitzsimmons, T. Z. Ward, and G. Eres for feedback on an early version of this manuscript. We also thank H. Liu, L. Yin, and J. Shen from Fudan University for assistance with magnetic force microscopy experiments and L. Debeer-Schmitt of the High Flux Isotope Reactor at Oak Ridge National Laboratory for assistance with small-angle neutron scattering experiments. **Funding:** This work was supported by the U.S. Department of Energy (DOE), Basic Energy Sciences, Materials Sciences and Engineering Division. Use of the Advanced Photon Source and the Advanced Light Source, which are DOE Office of Science User Facilities, was supported by DOE's Office of Science under contracts DE-AC02-06CH11357 and DE-AC02-05CH11231, respectively. The Hall effect measurements in high magnetic fields were performed at the NHMFL, which is supported by NSF cooperative agreement no. DMR-1644779 and the state of Florida. **Author contributions:** E.S., J.N., and H.N.L. designed the experiment and wrote the manuscript with input from all authors. E.S. and J.N. performed sample growth, Hall effect, and magnetometry measurements. J.M.O., E.S., and M.B. performed high magnetic field measurements at the NHFML with the support of E.S.C. R.V.C. performed XMCD-PEEM measurements and analysis at the ALS. A.R. and C.S. provided assistance with sample growth and electronic transport measurements. E.S., J.N., C.S., and R.D.D. performed hard and soft x-ray absorption experiments and analysis with the support of Y.C., D.H., and J.W.F. at the APS. X.G. and S.Y. were responsible for STEM measurements and analysis. T.F. and J.N. carried out micromagnetic simulations, and S.O. carried out theoretical simulations. **Competing interests:** The authors declare that they have no competing interests. **Data and materials availability:** All data needed to evaluate the conclusions in the paper are present in the paper and/or the Supplementary Materials. Additional data related to this paper may be requested from the authors.

Submitted 5 September 2019
Accepted 22 May 2020
Published 3 July 2020
10.1126/sciadv.aaz3902

Citation: E. Skoropata, J. Nichols, J. M. Ok, R. V. Chopdekar, E. S. Choi, A. Rastogi, C. Sohn, X. Gao, S. Yoon, T. Farmer, R. D. Desautels, Y. Choi, D. Haskel, J. W. Freeland, S. Okamoto, M. Brahlek, H. N. Lee, Interfacial tuning of chiral magnetic interactions for large topological Hall effects in $LaMnO_3/SrIrO_3$ heterostructures. *Sci. Adv.* **6**, eaaz3902 (2020).

ScienceAdvances

Interfacial tuning of chiral magnetic interactions for large topological Hall effects in $LaMnO_3$/$SrIrO_3$ heterostructures

Elizabeth Skoropata, John Nichols, Jong Mok Ok, Rajesh V. Chopdekar, Eun Sang Choi, Ankur Rastogi, Changhee Sohn, Xiang Gao, Sangmoon Yoon, Thomas Farmer, Ryan D. Desautels, Yongseong Choi, Daniel Haskel, John W. Freeland, Satoshi Okamoto, Matthew Brahlek and Ho Nyung Lee

Sci Adv **6** (27), eaaz3902.
DOI: 10.1126/sciadv.aaz3902

Science Advances (ISSN 2375-2548) is published by the American Association for the Advancement of Science, 1200 New York Avenue NW, Washington, DC 20005. The title *Science Advances* is a registered trademark of AAAS.